Journal of Nuclear Materials 590 (2024) 154873

Contents lists available at ScienceDirect

Journal of Nuclear Materials

journal homepage: www.elsevier.com/locate/jnucmat

Hydrogen enhanced localized plasticity in zirconium as observed by digital image correlation

Francesco Fagnoni [a,*], E . Cansu Kursun [a], Matteo Busi [b], Piotr Konarski [c], Okan Yetik [a,b], Ralph Spolenak [d], Johannes Bertsch [a], Liliana I. Duarte [a]

[a] Nuclear Energy and Safety, Laboratory for Nuclear Materials, Paul Scherrer Institut, CH-5232 Villigen PSI, Switzerland
[b] Research with Neutrons and Muons, Laboratory for Neutron Scattering and Imaging, Paul Scherrer Institut, CH-5232 Villigen PSI, Switzerland
[c] Nuclear Energy and Safety, Laboratory for Reactor Physics and Thermal-Hydraulics, Paul Scherrer Institut, CH-5232 Villigen PSI, Switzerland
[d] Laboratory for Nanometallurgy, Department of Materials, ETH Zurich, CH-8093, Zurich, Switzerland

ARTICLE INFO

Keywords:
HELP
DIC
Zr
Clad
Cladding
Hydrogen

ABSTRACT

Hydrogen embrittlement in zirconium alloys is a highly relevant research topic, important for ensuring the integrity of nuclear fuel clads. While the presence of hydrides in zirconium-based clad is a well-known risk factor due to their brittleness, the effect of the presence of hydrogen in solid solution is unclear.

According to the Hydrogen Enhanced Localized Plasticity (HELP) model, hydrogen in solid solution may affect the mechanical performance of a metal by increasing dislocation mobility due to the shielding effect that hydrogen has on the interaction of dislocations with other types of defects. In the presented work, the presence of HELP has been assessed in Zircaloy-4 samples, under conditions relevant to the storage of spent nuclear fuel.

Elevated temperature tensile tests were performed on samples containing localized areas of higher hydrogen concentration, as quantified by neutron radiography. Digital Image Correlation (DIC) analysis was performed on the specimen surfaces for quantitative characterization of strain heterogeneity during deformation to identify the regions where the plastic strain localization occurs.

These regions could be correlated to elevated amounts of hydrogen in solid solution, that is, in the location immediately adjacent to dissolving hydrides, or in the areas of the samples with local hydrogen concentration close to the expected terminal solid solubility limit (TSS) in the test conditions.

The results confirm the presence of localized softening caused by solid solution hydrogen, indicating that the HELP mechanism needs to be taken into account when modeling the mechanical response of zirconium-based nuclear fuel clads at elevated temperatures.

1. Introduction

In the area of interest for spent nuclear fuel storage, hydrogen can be found both in solid solution or in the form of hydrides [1]. In conditions below terminal solid solubility, the leading embrittlement mechanism is through cleavage across brittle hydrides (e.g. [2,3]); however, in conditions of high temperature and low hydrogen concentration, hydrogen is stable in solid solution inside the metal lattice. In such conditions, it is speculated that hydrogen enhances dislocation mobility, leading to increased ductility of the material.

This increased ductility has been extensively described for steels (e.g., [4–6]), however, it is unclear whether a similar mechanism is active in Zr alloys under conditions faced by spent nuclear fuel.

The hydrogen-induced softening effect is difficult to observe in zirconium alloys as it is often compensated by the more prominent effect of hardening due to hydrides. However, it cannot be discounted that the conditions necessary to activate the softening mechanism might be active locally within the clad e.g. in the vicinity of large hydrogen accumulations (especially in claddings containing a liner [7,8]).

The mechanical properties of zirconium alloys in the presence of a uniform distribution of low amounts of hydrogen have been recently published by Fagnoni et al. [9]. The results highlighted the presence of softening effects in the region where the majority of hydrogen is expected to be in solid solution. The effect of hydrogen in solid solution appears to be minor compared to the effect of hydrides, but significant, with the most pronounced softening effect recorded at 300 °C for

* Corresponding author.
E-mail address: francesco.fagnoni@psi.ch (F. Fagnoni).

https://doi.org/10.1016/j.jnucmat.2023.154873
Received 3 April 2023; Received in revised form 25 October 2023; Accepted 17 December 2023
Available online 18 December 2023

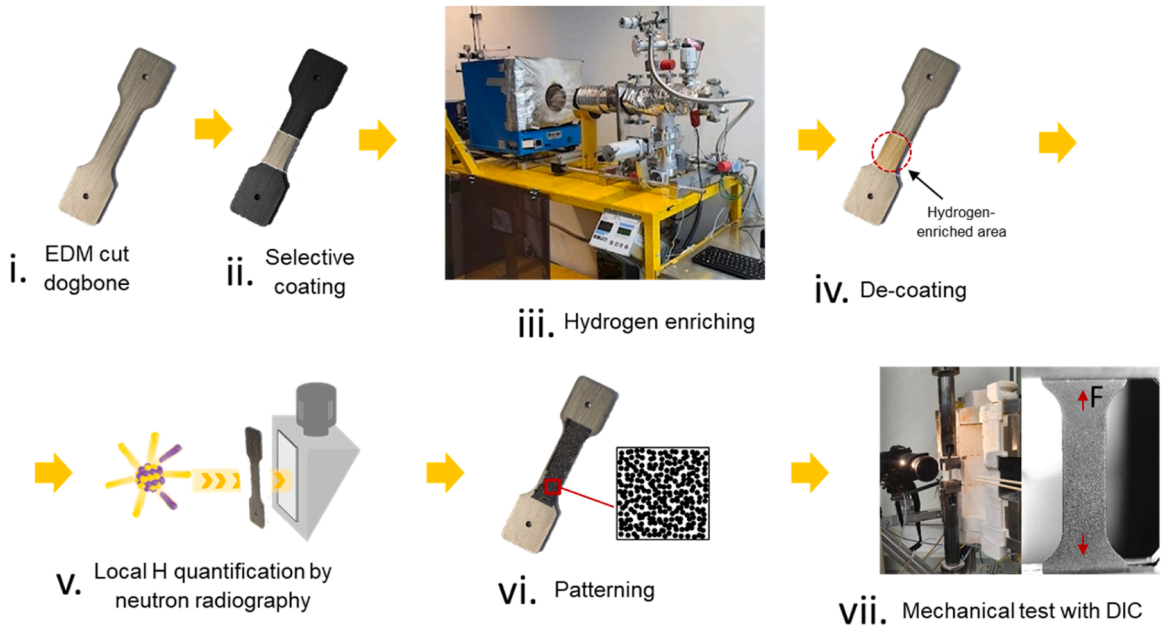

Fig. 1. Experimental methodology adopted. Dog-bone samples were prepared by EDM cutting (i). Subsequently, a selective coating was applied to promote localized hydrogen enrichment (ii). The samples were then exposed to a hydrogen-rich atmosphere in a Sieverts-type apparatus (iii), and the resulting hydrogen distribution within the sample was assessed by neutron imaging (iv),(v). Finally, a random pattern was applied to the gauge of the dog-bone to allow DIC analysis (vi), and the samples were subjected to tensile tests at elevated temperature.

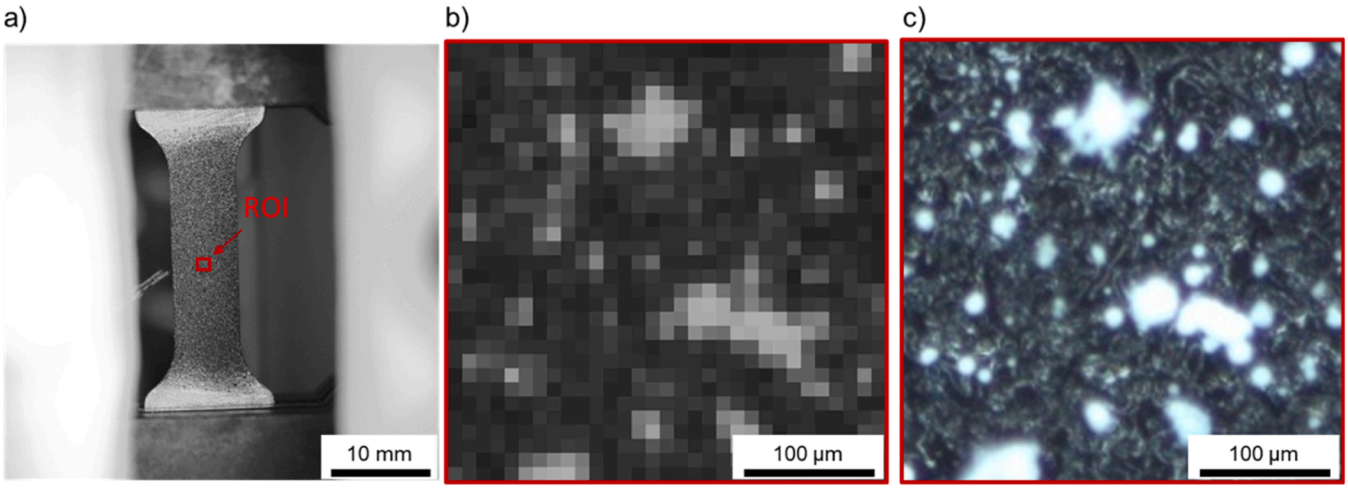

Fig. 2. Image acquired by the camera during in-situ testing (a), enlarged view of a region of interest (ROI) of the image used for DIC, illustrating the contrast resulting from the speckle distribution (b); corresponding optical microscope image of the ROI, illustrating the random speckle pattern (c). The ROI visualized is 31 × 31 pixels, corresponding to the subset size used for the DIC analysis.

Zircaloy-4 samples enriched with 100 wt ppm of hydrogen.

To study the effect that discrete sources of hydrogen have on the strain localization in zirconium, differentially enriched samples were subjected to tensile tests at elevated temperature. The distribution of the strain field during tensile testing was measured by digital image correlation (DIC) analysis. DIC is a non-contact, optical measurement technique that is becoming increasingly popular for measuring the deformation response of materials [10–12].

In this work, DIC analysis was conducted at elevated temperatures during tensile tests to identify the effect of hydrogen distribution on plastic strain localization. The measured strain fields were compared to the hydrogen distribution within the samples as spatially quantified prior to the test by non destructive neutron imaging [7,8,13,14].

DIC showed substantial strain concentration in areas adjacent to highly charged ones, and generalized strain localization in the presence of hydrogen amounts close to the solid solubility limit, confirming the presence of a hydrogen induced softening mechanism in zirconium.

2. Methods

For the project, a 2.5 mm thick Zircaloy-4 recrystallized sheet was supplied by Framatome.

Samples used for mechanical tests were produced from allocated samples by water-jet cutting. The dog-bone gauge was 18 mm long and 7 mm wide, with a connecting radius of 6 mm. The machining process allowed for tolerances of ±0.02 mm.

The Zircaloy-4 composition, according to the ASTM B351/B351M-13 (2018) standard is: tin 1.20–1.70 wt.%, iron 0.18–0.24 wt.%, chromium 0.07–0.13 wt.%, and other impurities in concentrations <0.05 wt.%. The microstructure of the base material had an average grain size of 5

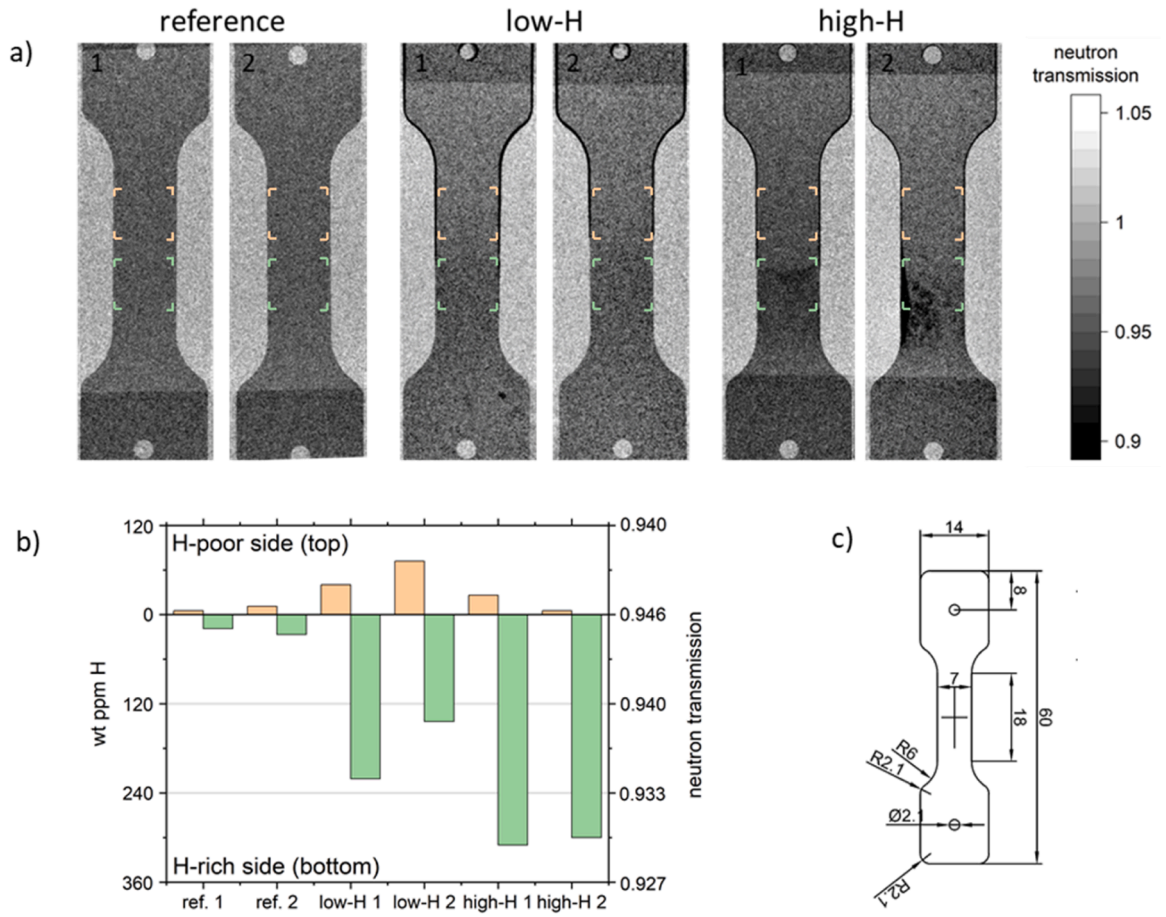

Fig. 3. (a) Neutron transmission images of the prepared samples before mechanical testing. A darker contrast corresponds to a higher hydrogen content, due to the higher attenuation cross section of hydrogen compared to Zr. The darker contrast at the grips of the samples is due to the aluminum tape used to attach the samples and does not influence the analysis in the gauge area. (b) Average hydrogen concentration determined in the sampling area between 2 mm and 6 mm from the gauge mid-line, shown in the sub-figure a. The hydrogen-poor side of the samples has hydrogen concentration lower than the expected TSSD at the testing temperature (120 wppm at 350 °C) whereas the hydrogen-rich side of the samples possess hydrogen concentration between TSSD and TSSP (240 wppm at 350 °C) in the samples *low-H* and above TSSP in the samples *high-H*. (c) Sample dimensions, in mm. The sample thickness is 2.5 mm.

μm and preferential 0001 orientation along the normal direction, with some tilt towards the transverse direction, as confirmed by EBSD measurements [15].

Fig. 1 represent schematically the experimental procedure adopted. To manifest the hydrogen enhanced localized plasticity (HELP) effect, the samples were charged with hydrogen. Diffusion of high purity hydrogen following high vacuum conditions was employed, following a similar procedure to the one described in [16].

For optimal hydrogen charging, samples were first polished using 2000 grit silica abrasive paper. Post-polishing, they were cleaned in acetone and then treated to a 3-minute ultrasonic bath in ethanol to ensure thorough cleanliness. After air-drying, the samples were accurately weighed on a precision balance.

To obtain the desired hydrogen gradient within the samples, half of the sample was coated prior to hydrogenation with heat resistant silicon paint to prevent hydrogen absorption into the metal in the coated area.

In the hydrogenation phase, samples were placed in a high-vacuum environment (10^−7 mbar) at room temperature for 12 hours. The system underwent three cycles of hydrogen flushing at 100 mbar, with high-vacuum restoration after each. The temperature was subsequently raised to 400 °C and held for 24 hours. The hydrogenation level was controlled through the formula

$$C_r = K\frac{p_I - p_E}{m_s}$$

where C_r is the target hydrogen concentration, m_s represents the sample weight, p_I and p_E are the starting and final hydrogen pressures, and K is an experimental constant assumed to be equal to 660.

The sample was subsequently de-coated by mechanically grinding both faces of the samples with 600 grit paper prior to assessing the resulting hydrogen distribution within the sample by neutron imaging.

Transmission contrast neutron images of the samples were acquired at the BOA cold neutron beamline [17] of the Swiss spallation neutron source [18] at the Paul Scherrer Institut (Switzerland). The imaging detector consisted of a 100 μm thick (LiF/ZnS(Ag)) scintillator screen and an optical Andor iKon-L CCD camera (2048 × 2048 pixels) equipped with a Zeiss MAKRO-PLANAR 2/100 mm ZF.2 objective lens. The magnification of the lens was such to achieve a field of view of 96 × 96 mm^2 thus, an effective pixel size of 47 μm. In order to have optimal image resolution, the samples were attached to the scintillator screen, from the head and the tail of the dog-bone, with aluminum tape.

The hydrogen concentration within the sample was estimated adapting the calibration obtained by Gong et al. [7] to 2.5 mm plate material, obtaining hydrogen sensitivity of 2.1 ± 0.1 cm^{-1}/wt ppm H.

Mechanical tests were performed using a 10 kN MTS universal tensile machine equipped with an environmental chamber and contact extensimeter. The samples were subjected to tensile test in the transversal (rolling) direction. The tensile tests were conducted with displacement control, imposing crosshead movement of 0.5 mm/min until fracture. The temperature during the tests was set to 350 °C. Testing conditions

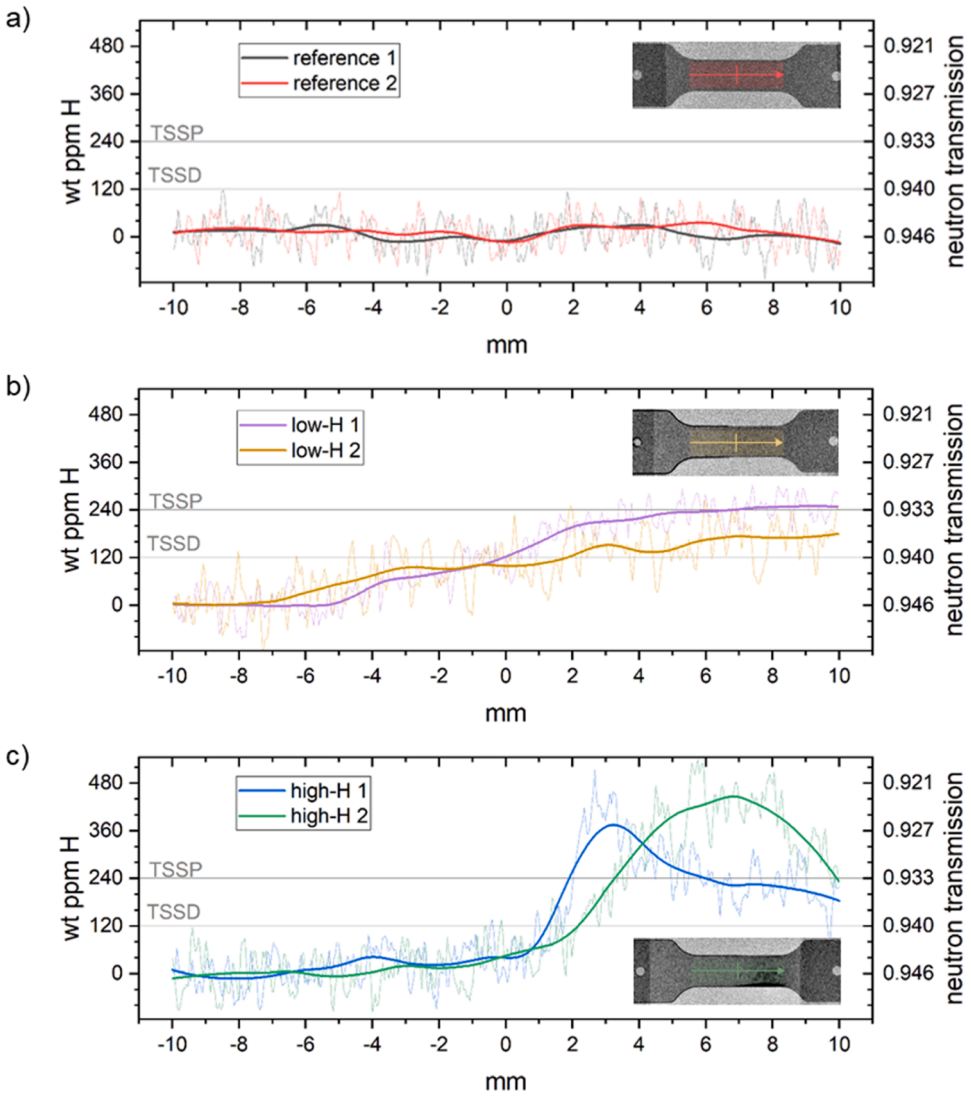

Fig. 4. Linear neutron transmission profiles and corresponding estimated hydrogen concentration obtained along the lenght of the gauge. The measurements are referenced to 0 mm at the center of the specimen. The neutron transmission profiles of the reference samples, *low-H* samples (possessing low hydrogen gradient), and *high-H* samples (possessing sharp hydrogen gradient) are reported in the sub-figures a), b), and c) respectively.

were reached after 10 °C/min heating, and a hold time of 30 minutes for the hydrogen-free samples, and 180 minutes for the hydrated samples. The temperature was monitored using a thermocouple sded to the specimen. After sample rupture, the necking position and fracture surface were measured with an optical microscope.

The total hydrogen distribution and solid solution fraction expected within the sample at the beginning of the tensile test can be calculated from the initial conditions assessed by neutron radiography, applying concentration-gradient diffusion during heating-up and dwell time at test temperature. Simulations were performed using an in-house developed finite volume solver. The dissolution and precipitation of hydrides were simulated with the hydride nucleation-growth-dissolution (HNGD) model [19]. Since the temperature gradient within the sample was absent, the only driving force for hydrogen flux J_h is the hydrogen concentration gradient in solid solution ∇c_{SS}:

$$J_h = D\nabla c_{SS}, \tag{1}$$

where the diffusion coefficient D is given by [20]:

$$D = 7.9 \times 10^{-7} \exp\left(\frac{-4.49 \times 10^4}{RT}\right)\left[m^2 s^{-1}\right], \tag{2}$$

where R $[Jmol^{-1}K^{-1}]$ in Eq. (2) is the gas constant, and $T[K]$is temperature. The HNGD model requires specifying the terminal solid solubility for dissolution (TSSD) and precipitation (TSSP). In this work, the correlations derived by Kammenzind et al. are used [21]:

$$\text{TSSD} = 66000 \exp\left(\frac{-32177}{RT}\right)[\text{wt ppm H}], \tag{3}$$

$$\text{TSSP} = 31000 \exp\left(\frac{-25264}{RT}\right)[\text{wt ppm H}]. \tag{4}$$

The test was monitored with a Canon EOS 200D camera through a small opening into the test chamber. To perform DIC analysis at elevated temperatures, heat resistant black and white vinyl-based paints were used to generate speckle patterns on the specimen surfaces. The specimen surfaces were covered with black paint as a background, and white paint was applied to generate white speckle distributions. The applied speckle pattern had a strong optical contrast and could withstand high temperature environments up to 500 °C. The diameter of the resulting speckles, as viewed by the DIC camera, were ~ 30–50 μm. The images for DIC analysis were acquired using a Canon EOS 200D camera at the standard image resolution 2048 pixels x 2048 pixels.

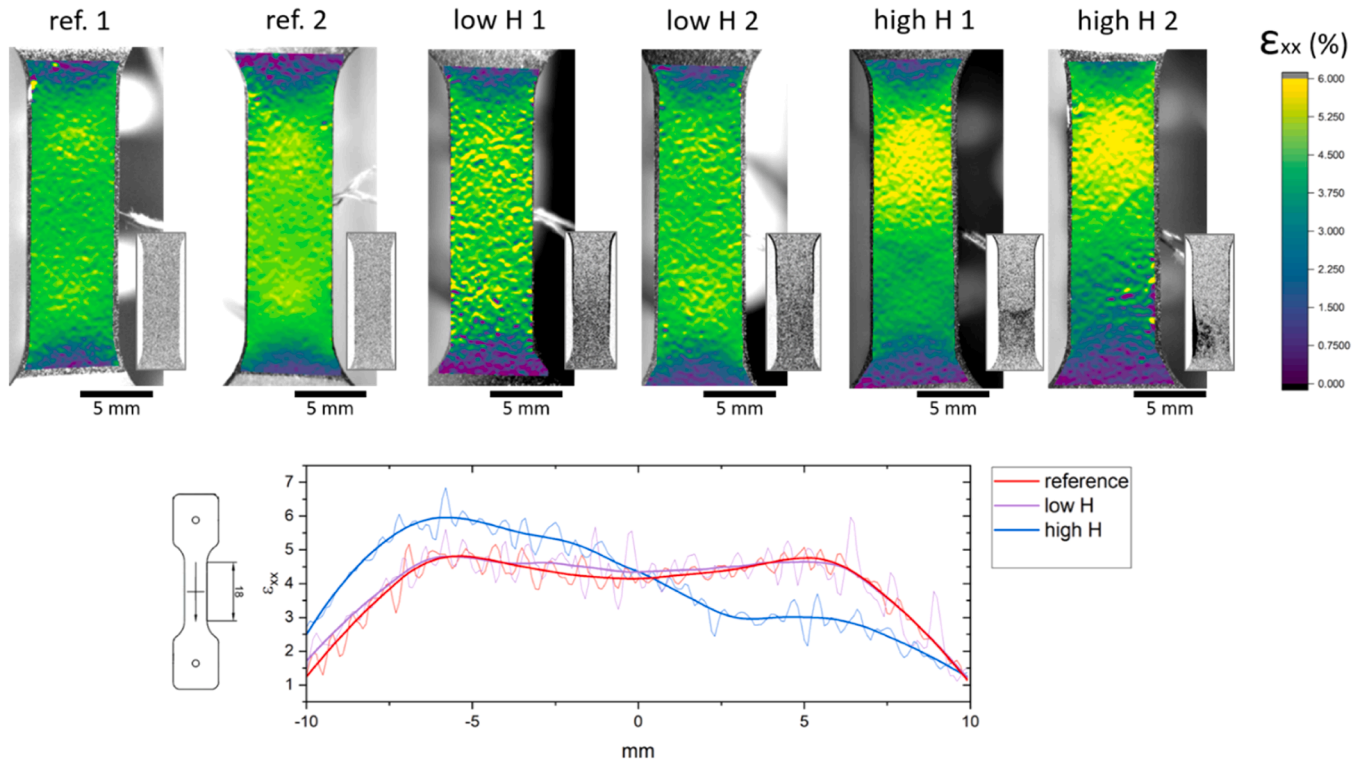

Fig. 5. Strain maps along the direction of the tensile deformation (ϵ_{xx}) obtained by DIC at 3.5 % global strain of the tensile specimens. Hydrogen distribution maps from Fig. 3 are provided again in the small windows for convenient reference. A strong localization of strain is observed in the samples containing a high hydrogen gradient (*high-H*). The samples charged with lower amounts of hydrogen (*low-H*) present strain localization at the micro-level. Strain distribution in the reference material is comparatively uniform. The line-scans along the vertical mid-section of the tensile samples (average betwenn the 2 homologus) is presented at the bottom of the image.

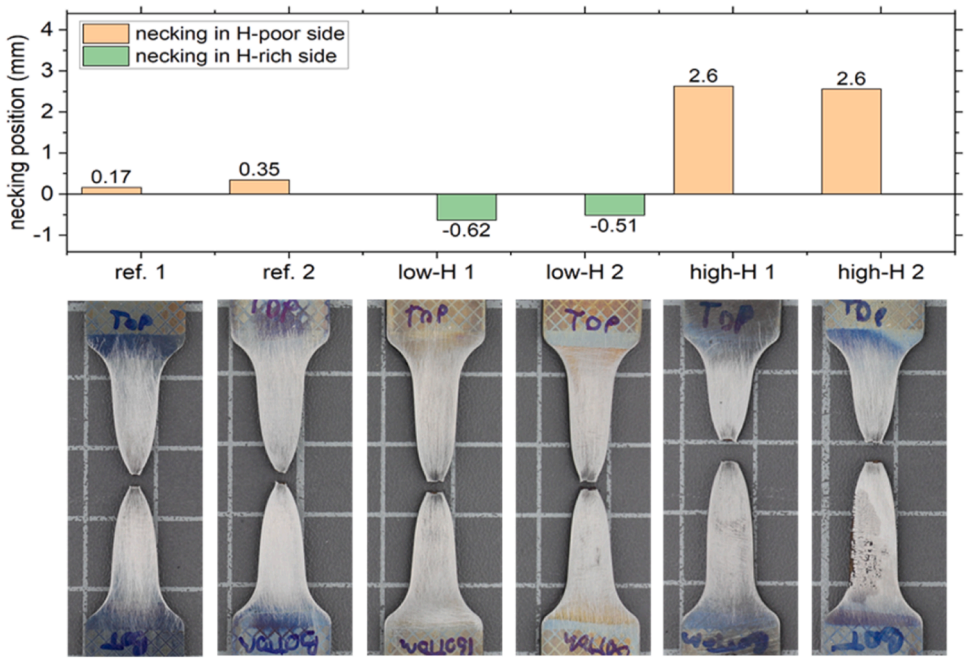

Fig. 6. Samples after tensile test at 350 °C. The position of the necking appears in the hydrogen-poor side in the *high-H* samples possessing large hydrogen gradient, and in the hydrogen-rich side in the samples *low-H* possessing hydrogen concentration closer to solid solubility. The necking position is central in the reference samples.

A view of the setup, with the environment chamber open, is shown in Fig. 1– vii. Fig. 2 shows an example of the image acquired during the imaging process, and the corresponding pattern. Pictures were taken at 5 s intervals during tensile deformation, corresponding to a picture every 83 μm of movement of the crosshead.

The images acquired in situ during tensile tests were subjected to DIC

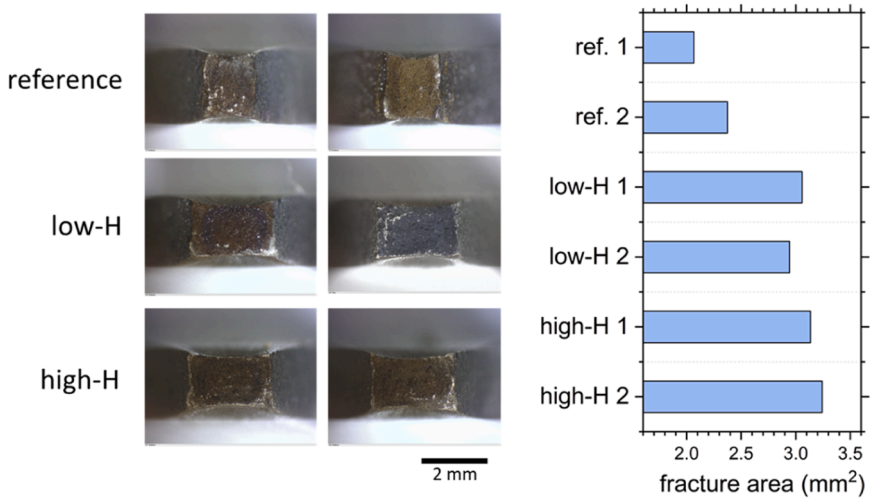

Fig. 7. Fractography images of the tested samples. Fracturing appeared after an 87 % reduction of the cross-section in the reference samples, and after an 83 % and 82 % reduction of the cross-sectional area in the *low-H* and *high-H* samples, respectively. The different aspect ratio of the hydrogen-rich samples compared to the reference is probably due to the influence of the orientation of the hydrides, that tend to precipitate preferentially on the basal (0001) plane [2], corresponding to the rolling plane of the specimens.

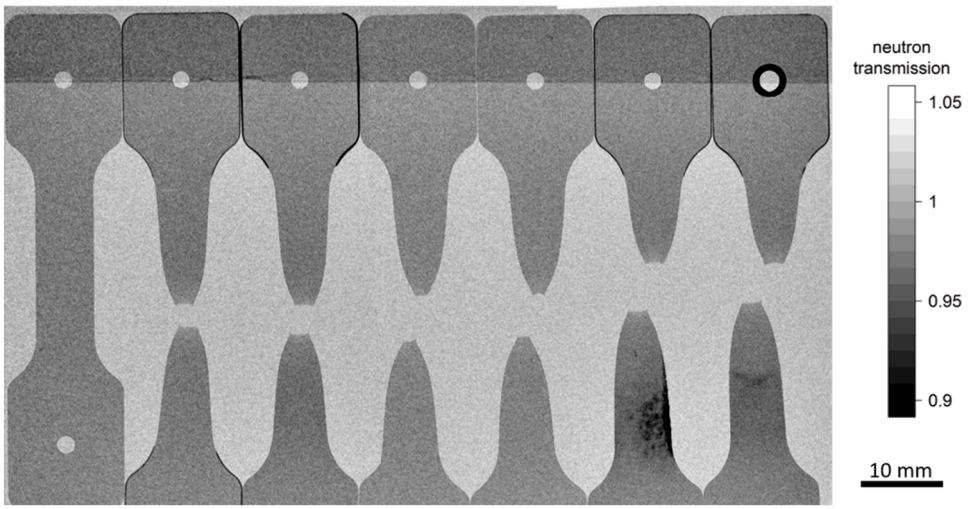

Fig. 8. neutron radiography image of the samples after test. From left to right, a reference sample in the as received state (without hydrogen addition), the samples low H2, low H1, reference 2, reference 1, high-H 2 and high-H.

analysis using VIC 2D 6 software (Correlated Solutions, Inc.) to obtain strain maps at different stages of deformation. In post-processing of the images, a 31 pixels × 31 pixels (corresponding to 465 um × 465 um) subset size and a 3 pixels (corresponding to 45 μm) step size were chosen. The size and distribution of the speckles in the speckle pattern were taken into consideration when choosing the dimensions of the subset to ensure that each subset had sufficient speckle distribution. During the strain computation, a 5 × 5 decay filter was selected as the minimum filter length required by the software to smooth the strain fields. The image processing was carried out until it reached approximately 5 % global strain whereupon paint delamination started on the specimen surfaces and the speckle pattern quality degraded. The images for DIC analysis were processed by using the image taken at the undeformed state as reference and processing all the images at the deformed state relative to the reference image by using Zero-mean normalized sum of squared differences (ZNSSD) as a correlation criteria. The global strains were estimated from the average value of strains computed by DIC on the gauge section of the specimens.

To assess the presence of localization of plasticity in presence of non-uniform hydrogen concentration, three categories of samples were employed in the presented study:

1. **Reference samples** (in the subsequent text referred as "***reference***"), consist of dog-bones obtained directly from the material in the as-received state. The hydrogen concentration in the base material was certified to be lower than 9 wt ppm H;
2. **Highly hydrogen enriched samples** (in the subsequent text referred as "***high-H***"), where a strong hydrogen gradient was created within the sample, leading to half of the sample being hydrogen-poor (<9 wt ppm H), and the other half having hydrogen well above TSSP at the test temperature (>240 wt ppm H at 350 °C [1]);
3. **Slightly enriched samples** (in the subsequent text referred as "***low-H***"), where half the sample was enriched to a hydrogen concentration between TSSD and TSSP at the test temperature (between 120 wt ppm H and 240 wt ppm H at 350 °C [1]), while maintaining the other half as hydrogen-free as possible.

Two samples per category were tested with the described

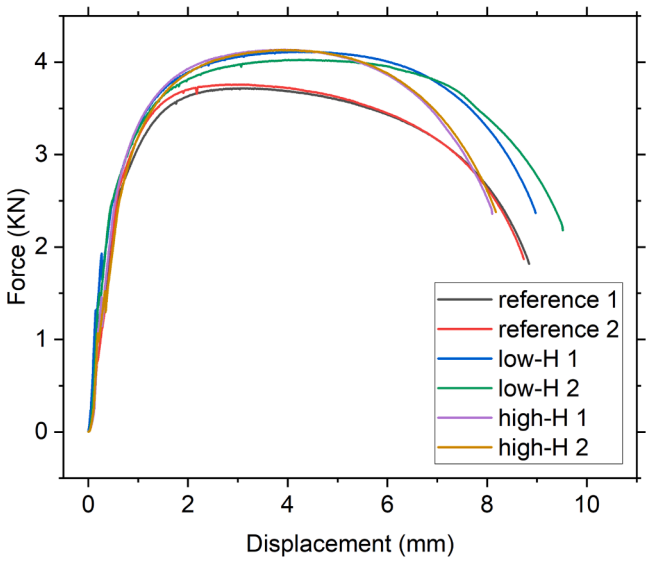

Fig. 9. Strain-Stress curve obtained during tensile test at 350 °C. The *reference* material represents the lower ultimate tensile strength (UTS), while the maximum elongation at rupture is reached by the samples containing lower hydrogen gradient (*low-H* samples).

Table 1
Strain at rupture (ε_{tot}), ultimate tensile strength (UTS) and toughness obtained from the stress-strain curves presented in Fig. 9.

	ε_{tot} (mm/mm)	UTS (MPa)	Toughness (J/m^3)
ref. 1	0.49	212.4	89.20
ref. 2	0.49	214.7	89.11
ref. average	**0.49**	**213.5**	**89.15**
low-H 1	0.50	234.9	102.93
low-H 2	0.53	230.0	106.72
low-H average	**0.51**	**232.4**	**104.83**
high-H 1	0.45	236.3	91.74
high-H 2	0.45	236.1	91.79
high-H average	**0.45**	**236.2**	**91.77**

methodology. Results and considerations are discussed in the following sections.

3. Results

The neutron images of the analyzed samples are provided in Fig. 3, and the corresponding neutron transmission profiles along the spine of the sample, referenced to the midpoint of the gauge, are plotted in Fig. 4.

The total hydrogen concentration within the gauge of the sample as measured by integration for the neutron transmission curves is: 8 wt ppm H and 14 wt ppm H for the *reference* samples, 126 wt pppm H and 99 wt ppm H for the *low-H* samples, 123 wt ppm H and 146 wt ppm H for the *high-H* samples.

Both the *high-H* samples present a well-defined hydrided area of macroscopic size, visible to the naked eye, formed during the hydrogen enrichment process. In all the hydrogen-enriched samples, the majority of the hydrogen is concentrated in the area of the gauge section that was uncoated during hydrogen pickup. Average hydrogen concentrations in the hydrogen-poor half of the gauge (coated during hydrogen pickup) and hydrogen-rich half of the gauge (uncoated during hydrogen pickup) are presented in Fig. 3b. In the *high-H* samples, the measured hydrogen concentration in the hydrogen-rich area of the sample exceeded TSSP at test temperature (above 240 wt ppm H), whereas in the *low-H* samples, the hydrogen concentration in the hydrogen-rich area is between TSSP and TSSD at the test temperature (between 120 wt ppm H and 240 wt ppm H). The hydrogen concentration measured in the hydrogen-poor area is below TSSD for all the samples.

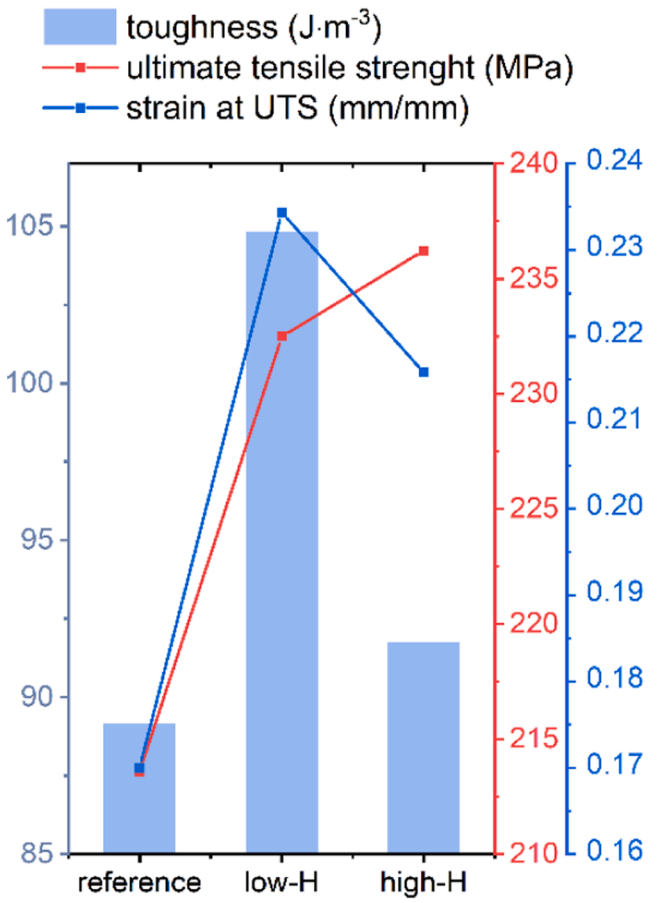

Fig. 10. Toughness, ultimate tensile strength (UTS) and strain at UTS recorded in the tested samples and averaged by category.

The hydrogen distribution profiles presented in Fig. 4 were produced applying a Loess smoothing, with span of 0.3. In the reference samples, the fluctuations in the estimated hydrogen concentration amounts to ±20 wt ppm H. As the neutron transmission is expected to be constant in the hydrogen-free sample, this measurement can be considered a good estimate of the measuring error of the technique.

Strain mapping obtained by DIC analysis at 3.5 % global strain during tensile tests at 350 °C is provided in Fig. 5. The results indicate a strong localization of the deformation in the hydrogen-poor area of the *high-H* samples with large dissolving hydrides. In the *low-H* samples, strain is comparatively more uniformly distributed, however, there are strong fluctuations in the recorded strain in regions of around 30 μm. The *reference* samples present a uniformly distributed strain along the full length of the gauge.

The test was conducted until rupture. In all the tested cases, the sample failed in a ductile way after 45–53 % elongation. Fig. 6 presents images of the samples after rupture, with the necking region highlighted. Necking appeared in the hydrogen-poor side of the *high-H* samples, whereas in the *low-H* samples, fracturing appeared towards the hydrogen-rich side. The reference samples broke within 0.35 mm from the mid-line. Fracturing appeared after an 87 % reduction of the cross-section in the *reference* samples, and after an 83 % and 82 % reduction of the cross-sectional area in the *low-H* and *high-H* samples respectively, as shown in Fig. 7. The hydrogen distribution in the samples was checked after the test once again by neutron imaging. The resulting image is presented in Fig. 8. Stress-strain curves are shown in Fig. 9. The ultimate tensile strength was considerably higher for the samples enriched with hydrogen compared to the reference samples. Both the elongation at rupture and the material toughness, considered one of the

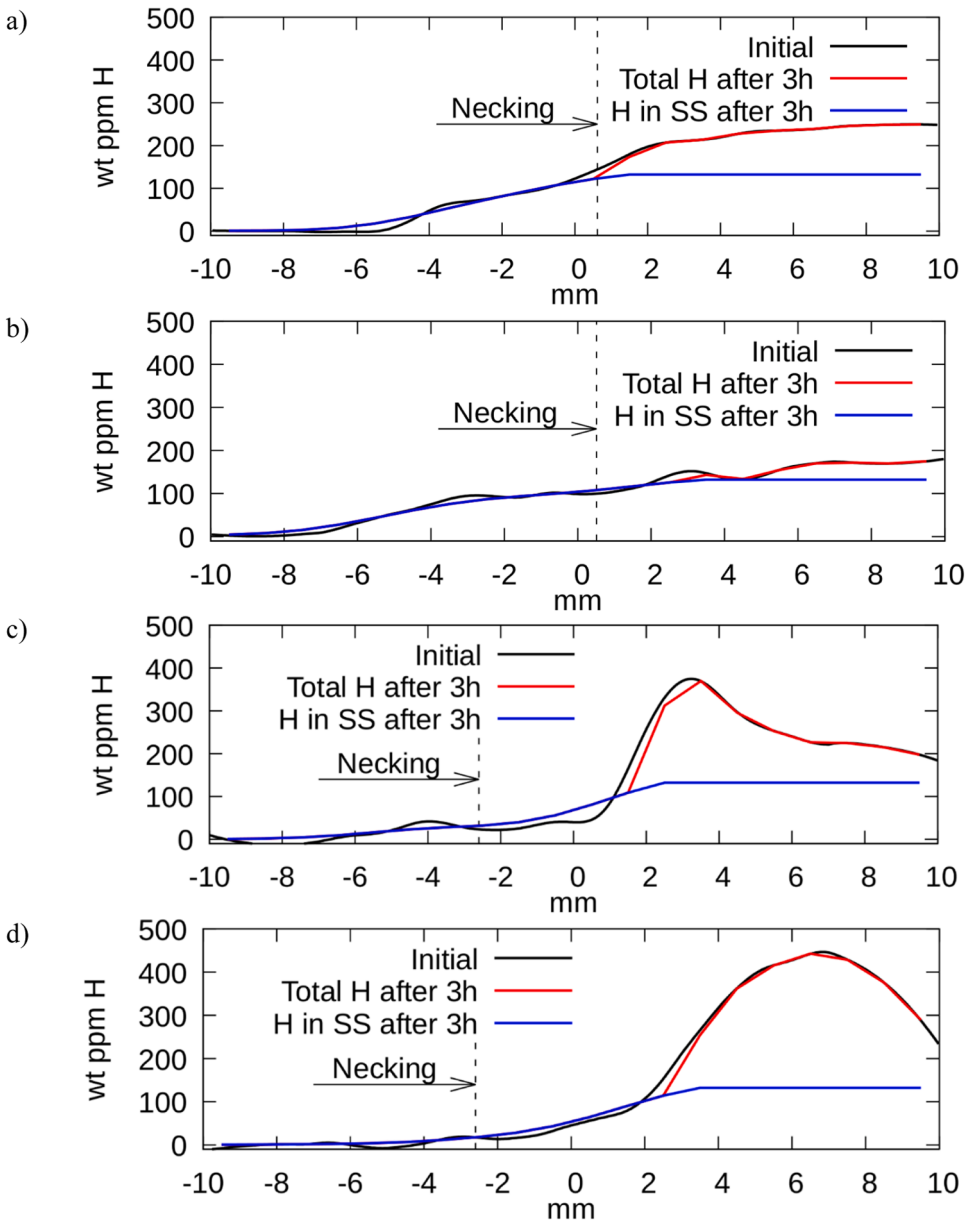

Fig. 11. Hydrogen concentration profiles in the samples: a) *low-H* 1, b) *low-H* 2, c) *high-H* 1, d) *high-H* 2. Black curves - total hydrogen concentration after hydrogenation, red curves – total hydrogen concentration after 3 h of dwelling at 350 °C prior to the mechanical test, blue curves – as the red ones but showing hydrogen in solid solution.

most important plasticity parameters, are significantly higher in the samples presenting higher amounts of hydrogen in solid solution (low-H). This can be further understood by examining the data in Table 1, where we see that the average UTS for low-H samples is approximately 9 % higher than the reference average, and their toughness, calculated as area under the stress-strain curve, is about 17.5 % greater than the reference samples. It is worth noting that high-H sample 1 and high-H sample 2 behaved remarkably similarly, despite the presence of strongly differing hydrogen distributions within the samples; this confirms that the deformation and failure mechanism is governed by the hydrogen-poor side (possibly with a contribution of hydrogen in solid solution). Fig. 10 further underscores this point; the UTS of high-H samples is slightly greater than that of the low-H samples, yet their toughness is almost comparable to the reference samples, being just marginally higher.

4. Discussion

The necking position can be correlated with the expected hydrogen distribution profiles to assess the influence of hydrogen in solid solution on the failure mechanism and softening behavior. The calculated hydrogen concentrations during tensile tests, taking into account hydride dissolution and hydrogen diffusion, are presented in Fig. 11. In the *low-H* samples, possessing a smooth hydrogen gradient, it is noted that fracturing appears close to where hydrogen in solid solution reaches a maximum, in the area directly adjacent dissolving hydrides (Fig. 11a and b). In the *high-H* samples, possessing a much sharper hydrogen gradient, the hardening effect due to large hydrides which force localization of strains towards the hydrogen-poor area of the sample, where necking and fracturing appears, possibly with a contribution of solid solution hydrogen, (Fig. 11c and d).

In the presence of high hydrogen concentration gradients within the sample, strain appears highly localized in the hydrogen-poor area of the

samples (Fig. 6 *high-H*). In the presence of smaller hydrogen gradients (Fig. 6 *low-H*), strain appears highly variable, with micro-regions possessing high deformation adjacent to micro-regions with low deformation. The same behavior is observed in both the hydrogen-rich and hydrogen-poor side of the samples, possessing total hydrogen concentration respectively above and below the expected TSSD at the testing temperature (120 wt ppm H at 350 °C). Therefore, the observed micro-localization of strain cannot be fully attributed to the presence of hydrides in the matrix, and the presence of hydrogen in solid solution must play a central role.

The total amount of hydrogen in solid solution expected during the test was determined from the simulations as 90 wt ppm H and 85 wt ppm H for the *low-H* samples and 73 wt ppm H and 66 wt ppm H for the *high-H* samples. Ultimate tensile strength (UTS) and sample toughness are both improved by the addition of hydrogen. However, while the UTS increases with increased hydrogen content, the sample toughness reaches a maximum in the samples containing the highest amounts of hydrogen in solid solution. Also, the elongation at rupture and strain at UTS appears to be larger in the samples possessing TSSP amounts of hydrogen in the system, indicating a correlation between hydrogen in solid solution and increased plasticity.

5. Conclusion

The main findings can be summarized as follows:

- Coating proved to be a successful method to control the hydrogen pickup to produce zirconium samples with a concentration gradient;
- Total elongation at fracture and sample toughness reaches a maximum in the specimens possessing higher amounts of hydrogen in solid solution;
- Digital image correlation analysis highlighted substantial strain localization in the areas directly adjacent to the highly charged ones in differentially charged samples subjected to tensile test at 350 °C;
- Micro-localization of stresses are observed in areas exhibiting hydrogen amounts below the solid solubility limit at the tested temperature;
- All samples failed in a ductile way; no cleavage across the hydride fraction was observed in samples possessing a macroscopic hydride section spanning the full width of the sample.

The results indicate strain localization in regions where elevated amounts of hydrogen in solid solution is expected, that is, in the region immediately adjacent to dissolving hydrides or in the areas of the samples with local hydrogen concentration close to the expected terminal solid solubility limit in the test conditions. The results imply that hydrogen in solid solution induces material softening in Zircaloy-4 samples, supporting the presence of HELP effect in zirconium alloys in conditions relevant for nuclear fuel cladding application.

CRediT authorship contribution statement

Francesco Fagnoni: Conceptualization, Data curation, Formal analysis, Investigation, Methodology, Validation, Visualization, Writing – original draft. **E . Cansu Kursun:** Data curation, Formal analysis, Investigation, Methodology, Validation, Visualization, Writing – review & editing. **Matteo Busi:** Data curation, Investigation, Methodology, Visualization, Writing – review & editing. **Piotr Konarski:** Data curation, Formal analysis, Investigation, Validation, Visualization, Writing – review & editing. **Okan Yetik:** Data curation, Formal analysis, Investigation, Methodology, Validation, Visualization, Writing – review & editing. **Ralph Spolenak:** Conceptualization, Data curation, Methodology, Project administration, Resources, Supervision, Writing – review & editing. **Johannes Bertsch:** Conceptualization, Data curation, Methodology, Project administration, Resources, Supervision, Writing – review & editing. **Liliana I. Duarte:** Conceptualization, Data curation, Methodology, Project administration, Resources, Supervision, Writing – review & editing.

Declaration of Competing Interest

The authors declare that they have no known competing financial interests or personal relationships that could have appeared to influence the work reported in this paper.

Data availability

Data will be made available on request.

Acknowledgments

This project has been financed by the Swiss Federal Nuclear Safety Inspectorate ENSI.

The authors would like to further acknowledge and express gratitude for this collaboration within the MIDAS program. The authors would also like to further acknowledge allocation of in-house beamtime at the BOA beamline of the SINQ, for the neutron imaging tests.

References

[1] A.T. Motta, L. Capolungo, L.-Q. Chen, M.N. Cinbiz, M.R. Daymond, D.A. Koss, E. Lacroix, G. Pastore, P.-C.A. Simon, M.R. Tonks, B.D. Wirth, M.A. Zikry, Hydrogen in zirconium alloys: a review, J. Nucl. Mater. 518 (2019) 440–460, https://doi.org/10.1016/j.jnucmat.2019.02.042.

[2] Y.-J. Jia, W.-Z. Han, Mechanisms of hydride nucleation, growth, reorientation, and embrittlement in zirconium: a review, Materials (Basel) 16 (2023) 2419, https://doi.org/10.3390/ma16062419.

[3] A.W. Colldeweih, F. Fagnoni, P. Trtik, R. Zubler, M.A. Pouchon, J. Bertsch, Delayed hydride cracking in Zircaloy-2 with and without liner at various temperatures investigated by high-resolution neutron radiography, J. Nucl. Mater. 561 (2022), 153549, https://doi.org/10.1016/j.jnucmat.2022.153549.

[4] H.K. Birnbaum, P. Sofronis, Hydrogen-enhanced localized plasticity—a mechanism for hydrogen-related fracture, Mater. Sci. Eng. 176 (1994) 191–202, https://doi.org/10.1016/0921-5093(94)90975-X.

[5] M.B. Djukic, G.M. Bakic, V. Sijacki Zeravcic, A. Sedmak, B. Rajicic, The synergistic action and interplay of hydrogen embrittlement mechanisms in steels and iron: localized plasticity and decohesion, Eng. Fract. Mech. 216 (2019), 106528, https://doi.org/10.1016/j.engfracmech.2019.106528.

[6] P. Gong, I.H. Katzarov, J. Nutter, A.T. Paxton, W.M. Rainforth, The influence of hydrogen on plasticity in pure iron—theory and experiment, Sci. Rep. 10 (2020) 10209, https://doi.org/10.1038/s41598-020-66965-z.

[7] W. Gong, P. Trtik, A.W. Colldeweih, L.I. Duarte, M. Grosse, E. Lehmann, J. Bertsch, Hydrogen diffusion and precipitation in duplex zirconium nuclear fuel cladding quantified by high-resolution neutron imaging, J. Nucl. Mater. 526 (2019), 151757, https://doi.org/10.1016/j.jnucmat.2019.151757.

[8] L.I. Duarte, F. Fagnoni, R. Zubler, W. Gong, P. Trtik, J. Bertsch, Effect of the inner liner on the hydrogen distribution of zircaloy-2 nuclear fuel claddings, J. Nucl. Mater. 557 (2021), 153284, https://doi.org/10.1016/j.jnucmat.2021.153284.

[9] F. Fagnoni, A. Colldeweih, S. Binato, J.M. Wheeler, R. Spolenak, M. Wolff, J. Bertsch, L. Duarte, Mechanical Behaviour of Zircaloy-4 in the Presence of Hydrogen in Solid Solu-Tion At Elevated Temperatures, ASTM, Ottawa, Canada, 2022.

[10] A. Weidner, H. Biermann, Review on strain localization phenomena studied by high-resolution digital image correlation, Adv. Eng. Mater. 23 (2021), 2001409, https://doi.org/10.1002/adem.202001409.

[11] B. Pan, K. Qian, H. Xie, A. Asundi, Two-dimensional digital image correlation for in-plane displacement and strain measurement: a review, Meas. Sci. Technol. 20 (2009), 062001, https://doi.org/10.1088/0957-0233/20/6/062001.

[12] H. Schreier, J.-J. Orteu, M.A. Sutton, Image correlation for shape, motion and deformation measurements: basic concepts, theory and applications, Springer US, Boston, MA, 2009. https://doi.org/10.1007/978-0-387-78747-3.

[13] M. Grosse, E. Lehmann, P. Vontobel, M. Steinbrueck, Quantitative determination of absorbed hydrogen in oxidised zircaloy by means of neutron radiography, Nucl. Instrum. Methods. Phys. Res. A 566 (2006) 739–745, https://doi.org/10.1016/j.nima.2006.06.038.

[14] M. Grosse, N. Kardjilov, Which resolution can be achieved in practice in neutron imaging experiments? – A general view and application on the Zr - ZrH2 and ZrO2 - ZrN systems, Phys. Procedia 88 (2017) 266–274, https://doi.org/10.1016/j.phpro.2017.06.037.

[15] F. Fagnoni, L.I. Duarte, J.M. Wheeler, J. Bertsch, Elevated temperature nanoindentation of Zry-4 in the presence of hydrogen in solid solu-tion, in: Santander (Spain), n.d.

[16] F. Fagnoni, P. Konarski, Hydrogen degassing of zirconium under high-vacuum conditions, Metals (Basel) 12 (2022) 868, https://doi.org/10.3390/met12050868.
[17] M. Morgano, S. Peetermans, E.H. Lehmann, T. Panzner, U. Filges, Neutron imaging options at the BOA beamline at Paul Scherrer Institut, nuclear instruments and methods in physics research section a: accelerators, spectrometers, Detectors Assoc. Equip. 754 (2014) 46–56, https://doi.org/10.1016/j.nima.2014.03.055.
[18] B. Blau, K.N. Clausen, S. Gvasaliya, M. Janoschek, S. Janssen, L. Keller, B. Roessli, J. Schefer, P. Tregenna-Piggott, W. Wagner, O. Zaharko, The swiss spallation neutron source SINQ at Paul Scherrer Institut, Neutron News 20 (2009) 5–8, https://doi.org/10.1080/10448630903120387.
[19] F. Passelaigue, E. Lacroix, G. Pastore, A.T. Motta, Implementation and validation of the hydride nucleation-growth-dissolution (HNGD) model in BISON, J. Nucl. Mater. 544 (2021), 152683, https://doi.org/10.1016/j.jnucmat.2020.152683.
[20] J.J. Kearns, Diffusion coefficient of hydrogen in alpha zirconium, Zircaloy-2 and Zircaloy-4, J. Nucl. Mater. 43 (1972) 330–338, https://doi.org/10.1016/0022-3115(72)90065-7.
[21] B.F. Kammenzind, D.G. Franklin, H.R. Peters, W.J. Duffin, Hydrogen pickup and redistribution in alpha-annealed zircaloy-4, ASTM STP 1295 (1996) 338–370.